Optics Letters

Multiperiodic magnetoplasmonic gratings fabricated by the pulse force nanolithography

Savelii V. Lutsenko,[1,*] Mikhail A. Kozhaev,[2,3] Olga V. Borovkova,[1,2] Andrey N. Kalish,[1,2,4] Alexei G. Temiryazev,[5] Sarkis A. Dagesyan,[1] Vladimir N. Berzhansky,[3] Alexander N. Shaposhnikov,[6] Alexei N. Kuzmichev,[2] and Vladimir I. Belotelov[1,2,3]

[1]Faculty of Physics, Lomonosov Moscow State University, Leninskie Gory, Moscow 119991, Russia
[2]Russian Quantum Center, Skolkovskoe shosse 45, Moscow 121353, Russia
[3]V. I. Vernadsky Crimean Federal University, Vernadsky Ave. 4, Simferopol 295007, Russia
[4]NTI Center for Quantum Communications, National University of Science and Technology MISiS, Leninsky Prospekt 4, Moscow 119049, Russia
[5]Kotel'nikov Institute of Radioengineering and Electronics of RAS, Fryazino Branch, Vvedensky Sq. 1, Fryazino 141190, Russia
[6]Research Center for Functional Materials and Nanotechnologies, Institute of Physics and Technology, V. I. Vernadsky Crimean Federal University, Vernadsky Ave. 4, Simferopol 295007, Russia
*Corresponding author: savlucenko@yandex.ru

Received 7 June 2021; revised 17 July 2021; accepted 21 July 2021; posted 29 July 2021 (Doc. ID 433309); published 20 August 2021

We propose a novel, to the best of our knowledge, technique for magnetoplasmonic nanostructures fabrication based on the pulse force nanolithography method. It allows one to create the high-quality magnetoplasmonic nanostructures that have lower total losses than the gratings made by the electron-beam lithography. The method provides control of the surface plasmon polaritons excitation efficiency by varying the grating parameters such as the scratching depth or the number of scratches in a single period. The quality of the plasmonic gratings was estimated by means of the transverse magneto-optical Kerr effect that is extremely sensitive to the finesse of a plasmonic structure.

https://doi.org/10.1364/OL.433309

Nowadays, magneto-optical (MO) techniques for the control of light attract significant interest [1]. Magnetic field allows manipulating optical parameters such as intensity and polarization at a high speed. Thus, MO effects are considered for telecommunication applications and are widely used for optical isolators, magnetic field sensors, biosensors, and data recording [2–8]. Some materials that do not reveal a strong intrinsic MO response are still rather attractive for these applications since the MO effects in them can be enhanced by the excitation of the optical modes, such as waveguide modes, localized and propagating surface plasmons [9–20]. The latter can be excited, for example, in the patterned magnetic heterostructures [14]. We can recall periodic subwavelength gratings of noble metals (Au, Ag), as well as the combined noble-magnetic gratings used for the enhancement of MO effects.

For the efficient excitation of the propagating surface plasmon polaritons (SPPs), it is necessary to fabricate the magnetoplasmonic nanostructures of proper geometry and size. Until now, several techniques have been applied for this purpose [21–31]. Usually, the electron-beam lithography (EBL) method is used since it provides a high resolution up to 10 nm and versatile pattern formation [25]. In the direct writing EBL, a small spot of the electron beam is written directly onto a resist coated substrate. The resulting nanostructured resist is used as a mask for subsequent layers applied to the sample.

Another method is nanoimprinting lithography with a resolution pattern of 2 nm and a density range of 10^{12} dots/cm^2. However, it has some critical issues that need to be addressed for the further progress of this technology, and of those, the most important are its limitations in handling complex patterns with varied feature density, patterning over topographies, and pattern alignment [29].

Also, a high-quality structure can be produced by etching a material using focused ion beams. Its advantage is that the mean square surface roughness is around 0.3 nm. But the essential drawback is the uncontrolled effect that ions have on the material; therefore, the properties of the material may be distorted. In addition to this, the production time is directly related to the energy of the ions [26].

Another noteworthy technique is vacuum annealing for nanoisland structures formation [23,24]. The size and location of the "islands" depend on the time and temperature of the vacuum annealing. Thereby it is possible to create an interaction between localized and propagating plasmon modes. However, this approach does not provide the fine control of the resulting parameters. In addition, the annealing speed depends on the applied temperature, and for fast, efficient creation of structures, it is required to maintain temperatures of the order of 1,000°.

There are two main types of laser-induced periodic surface structures (LIPSS), also known as ripples. Coarse or low spatial frequency ripples have a period close to the wavelength of the laser irradiation and a direction perpendicular to its polarization. The fine or high spatial frequency ripples, with a period much smaller than the irradiation wavelength, have a direction

parallel to the polarization vector. But it is difficult to create a desirable shape, especially since the characteristic parameters of structures made using by LIPSS are of the order of a micron [30,31].

In this Letter, we propose a new method for the fabrication of magnetoplasmonic structures based on a pulse force nanolithography method (PFNL) [22] (Supplement 1). It employs a rapid indentation of the sharp tip from one point to another with the help of a single crystal diamond tip. This approach provides a deep nanopatterning with high resolution in solid materials, like metals. The PFNL method allows us to fine-tune the geometry of the structure providing an excitation of SPP modes with higher quality. We address the structures fabricated by the PFNL method in terms of the MO properties. The PFNL structures are compared with the ones made by the EBL method.

We consider samples, each composed of a dielectric magnetic layer covered with metal grating that supports an excitation of the propagating SPP modes and waveguide modes in the layer. A 4-μm-thick magnetic dielectric film of bismuth-substituted iron garnet (BIG, $(YBi)_3(FeAlSc)_5O_{12}$) was grown on the gadolinium gallium garnet ($Gd_3Ga_5O_{12}$) substrate by the liquid phase epitaxy method. Then, a gold layer of $d = 40$ nm thickness was deposited on top of it by the magnetron sputtering method. Next, the gold layer was scratched by the PFNL method [see Fig. 1(a)] [22]. Gratings of 131 blocks with a period $P = 690$ nm were created in the sample. Each block is an array of several parallel grooves about 15 nm wide surrounded by hills of squeezed gold made by means of the nanolithography. The addressed structures are characterized by the distance between the lines in one block, p, and the number of lines in a single block, n. Two gratings 100 × 100 μm in size were made with different groove densities in a block. Parameters of the first structure (denoted here and further as "A") are $p = 75$ nm, $n = 5$, and the second structure (denoted as "B") are $p = 100$ nm, $n = 4$. In Fig. 1(b) are images of the structure "B" made by atomic force microscopy (AFM). Block sizes in both structures were approximately the same.

Moreover, the EBL structure (denoted as "E") [Fig. 2(b)] was made on the same sample for the comparison with the PFNL structure [Fig. 2(a)]. This "E" structure was fabricated as follows. First, a film of a sensitive polymer (electronic resist) was applied on top of the substrate. In our case, it was polymethyl methacrylate (950 PMMA A2) deposited by centrifugation. Gold film was formed by the magnetron sputtering in a direct current discharge in argon at a pressure of 5×10^{-3} mbar. For etching a gold film through a polymer mask, a conventional physical sputtering of the material in an argon discharge was used. Then, the remains of the polymer mask were removed

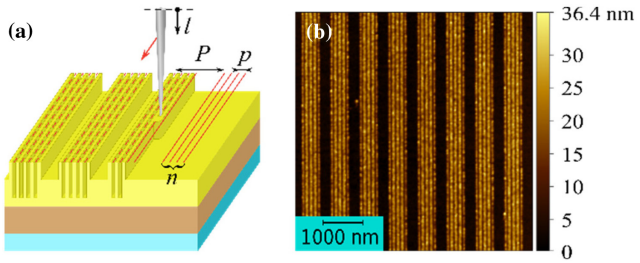

Fig. 1. (a) Scheme of the sample nanostructured by the PFNL technique. (b) Atomic force microscopy images of structure "B" made in tapping mode (Figs. S1 and S2). The zero-level corresponds to the intact surface of gold.

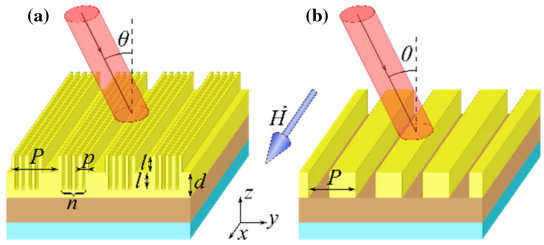

Fig. 2. Scheme of the samples and the optical measurements of (a) the PFNL structures "A", "B", and (b) the EBL structure "E".

using an oxygen plasma discharge. The period of this grating is $P = 690$ nm, the same as that of the PFNL structure. The width of the air gap is 115 nm; for the compared PFNL structures, it is 290 nm and 315 nm, respectively.

The scanning electron microscopy and AFM images of all structures "A," "B," and "E" are given in the Supplement 1 (Fig. S2).

The transverse MO Kerr effect (TMOKE) was measured to study the properties of the structures (for details see Supplement 1). It is determined by the relative change in the intensity of reflected light with magnetization **M** reversal $\delta = 2\frac{I(M)-I(-M)}{I(M)+I(-M)}$, where $I(\mathbf{M})$ is the intensity of the transmitted light in a magnetized state. Magnetization direction is perpendicular to the light incidence plane.

Magnetoplasmonic nanostructures support excitation of the various optical modes, in particular, the waveguide modes and propagating SPPs (for details, see Supplement 1). They can be revealed from the typical resonant features emerging in the transmission and the MO effect spectra (Fig. 3).

SPP modes at the gold-magnetic layer interface are seen in the experimental transmission and the TMOKE spectra in the form of a cross with a center of symmetry at zero incidence angle (green lines in Fig. 3). At the normal incidence, the SPP modes are excited at 760 and 775 nm in the PFNL gratings "A" and "B," respectively.

In Fig. 3 are the waveguide modes in the spectral range from 650 to 750 nm that show themselves as a set of crossing lines shifted from each other. Waveguide modes are excited up to 740 nm at normal incidence for both PFNL gratings [Figs. 3(a) and 3(b)], and at wavelengths up to 760 nm at normal incidence for the EBL grating [Fig. 3(c)]. Since the periods of structures

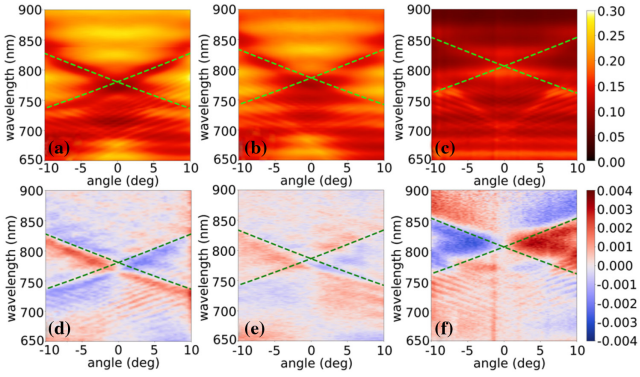

Fig. 3. (a)–(c) Experimental transmission and (d)–(f) the TMOKE spectra of "A" and "B" PFNL and "E" etched grating, accordingly. Green dashed lines correspond to the SPP resonances. The set of resonances in the range from 600 to 750 nm corresponds to the excitation of the waveguide modes in magnetic dielectric.

Table 1. Parameters of Resonances for the Investigated Structures at the Incidence Angle of 5°

	$\hbar\omega_p$ (eV)	λ_p (nm)	$\lvert q_p\rvert \times 10^{-3}$	$\hbar\gamma_p$ (eV)	$\hbar\gamma_z$ (eV)	$\hbar\omega_z$(eV)	λ_z (nm)
A	1.539 ± 0.001	806	3.9 ± 0.5	0.030 ± 0.001	0.025 ± 0.005	1.54 ± 0.01	805
B	1.526 ± 0.003	813	2.8 ± 0.8	0.032 ± 0.003	0.029 ± 0.006	1.53 ± 0.02	811
E	1.495 ± 0.003	829	67.4 ± 1.3	0.098 ± 0.002	0.194 ± 0.008	1.46 ± 0.02	847

"A," "B," and "E" are the same, the phase matching conditions turn to be similar. Therefore, both types of the nanostructures support the SPP modes of the same order in the same spectral range.

A distinctive feature of the SPP modes is their extremely high sensitivity to the properties of the metal/dielectric interface. This opens an opportunity to employ these modes as a quality studying tool for the plasmonic nanostructures (similarly to Ref. [18]).

Generally, the SPP resonance has the Fano resonance shape. The quality of the plasmonic nanostructures directly affects the parameters of the observed resonance. Comparing the resonance frequency, width, and Fano parameter for the nanostructures fabricated by two different methods, one can judge the capabilities of the particular method.

The intensity of the transmitted radiation in the spectral range of the SPP resonance can be written as [32]

$$\sim \frac{(\omega-\omega_z)^2+\gamma_z^2}{(\omega-\omega_p)^2+\gamma_p^2}|b_p|^2. \tag{1}$$

Here, ω_p is a resonance frequency ($\lambda_p = \frac{2\pi c}{\omega_p}$ is a central wavelength of the resonance), γ_p denotes total losses, $\omega_z = \omega_p[1 - \mathrm{Re}(q_p)]$, $\gamma_z = \gamma_p[1 - \frac{\omega_p}{\gamma_p}\mathrm{Im}(q_p)]$, and the corresponding wavelength is $\lambda_z = \frac{2\pi c}{\omega_z}$, b_p is a parameter characterizing the amount of radiation emitted by scattering from gratings, a_p characterizes the resonant processes, and $q_p = \frac{a_p}{\omega_p b_p}$ is a Fano parameter. The latter one shows what part of the field was subjected to the resonant process. Based on this, we can determine the efficiency of a system and its suitability for the excitation of modes of the structure, such as SPPs. Since the same set of modes was observed in all three structures, they can be compared. Table 1 contains the resonance parameters values found from the fitting of the observed experimental spectra based on Eq. (1).

The exact resonance position and shape depend on the grating geometry and are slightly different for PFNL and EBL gratings. First, one can observe the change in position of λ_p that occurs because the SPP arises at the interface between a dielectric and not continuous but a structured metal layer.

The shape of the resonance is specified by $|q_p|$ parameter. Indeed, the efficiency of the SPP excitation as well as the Fano parameter in neatly modulated structures "A" and "B" is lower than in the etched structure "E." Thus, for "A" and "B" structures, the resonance in the transmission spectrum is distinguished by a clearly pronounced transmission minimum, and by a maximum for "E" structure.

The quality factor of the resonance can be characterized by the resonance broadening $\hbar\gamma_p$. As can be seen from Table 1, the total losses of the PFNL structures are 3 times lower than in the etched structure. As it was shown earlier in Ref. [17] an increase of the Q-factor of the SPP resonances leads to the growth of the Q-factor of the corresponding magnetoplasmonic resonances. This can be clearly seen also in the TMOKE spectra in Figs. 3(d)–3(f), where the SPP resonance for "E" structure is apparently wider along the wavelengths axis.

The transmission and the TMOKE spectra for "A" and "B" structures are quite similar. The difference is bound to the resonance excitation efficiency $|q_p|$. This distinction can be seen from the TMOKE magnitude and is connected to the grooves number n.

To analyze MO properties of the PFNL structures, a rigorous coupled wave analysis was used [14]. The best agreement of simulated spectra with an experimental one is obtained if the scratching depth l and squeezed hills height were taken the same [Fig. 2(a)]. The transmission and the TMOKE spectra dependence on d were analyzed (Fig. 4). The following parameters were used: $P = 690$ nm, $p = 100$ nm, $n = 4$ (similar to "B" grating). To exclude the Fabry–Perot and the waveguide modes, the magnetic layer was considered semi-infinite. The excitation of the SPP modes was observed in the transmission and the TMOKE for $l \geq 25$ nm.

The resonance position λ_p shifts upward with the increase of the scratching depth l, as well as the parameter $|q_p|$ (Table 2). So, the resonance excitation efficiency depends on the scratching depth. Also, as shown in Fig. 4, the TMOKE increases with l. Therefore, varying the scratching depth and p parameter, one can change the key properties of the resonance. Detailed analysis of the impact of the scratched grooves and squeezed hills solely is given in Supplement 1.

It is also interesting to compare the simulated and experimental spectra. The TMOKE spectrum for simulated structure with $l = 25$ nm [Fig. 4(a)] is qualitatively the same as for "B" structure [Fig. 3(e)]. Despite the fact that for the modeled structure parameters p and n are the same as for "B" structure,

Table 2. Parameters of the Resonances for Simulated Structures Depending on the Depth of Scratching at 5° Incidence Angle

l (nm)	λ_p (nm)	$\lvert q_p\rvert \times 10^{-3}$	$\hbar\gamma_p$ (eV)	λ_z (nm)
25	790	2.2 ± 0.1	0.024 ± 0.005	789
30	798	2.7 ± 0.1	0.024 ± 0.005	798
35	818	3.3 ± 0.1	0.026 ± 0.005	817
40	824	5.4 ± 0.1	0.028 ± 0.005	825

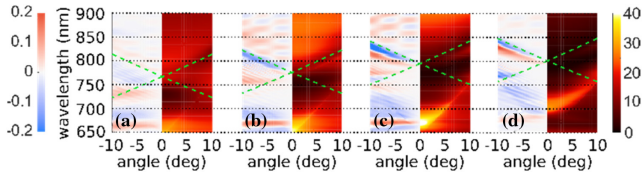

Fig. 4. (a) Simulated TMOKE and transmission spectra of the PFNL-type structures. Different grooves' depths are considered: $l = 25$, (b) 30, (c) 35, and (d) 40 nm.

there are also similarities in spectra for "A" structure. Thus, the TMOKE spectra for simulated structures with $l = 30,\ 35$ nm [Figs. 4(b) and 4(c)] are similar to the spectrum for "A" structure [Fig. 3(d)]. In other words, an increase in the number of scratches n acts as an increase of the scratch depth l. We can conclude that with the help of the proposed fabrication method, the result can be achieved either by varying the number of scratches or their depth. This expands the possibilities for setting a necessary configuration when fabricating structures.

To sum up, a novel method of plasmonic nanostructures fabrication was proposed. It is based on the pulse force nanolithography method. This technique provides a fine-tuning of the metal layer geometry and allows one to excite high-quality SPP modes. Indeed, the PFNL-made nanostructures demonstrate 3-times lower total losses of the SPP resonance with respect to the grating fabricated by the EBL and the concomitant increase of the quality of the magnetoplasmonic resonances. The proposed method provides opportunities for the control of the SPP excitation efficiency by varying the scratching depth or the number of scratches in a single period. The MO effect was employed to evaluate the quality of the fabricated gratings.

Funding. Russian Foundation for Basic Research (18-29-27020, 19-02-00856); Ministry of Science and Higher Education of the Russian Federation (075-15-2019-1934).

Acknowledgment. The equipment of the "Educational and Methodical Center of Lithography and Microscopy," Lomonosov MSU was used. A.N.K. and V.I.B. are members of the Interdisciplinary Scientific and Educational School of Moscow University "Photonic and Quantum technologies. Digital medicine." The authors are grateful for the assistance of V. V. Dremov with the AFM measurements.

Disclosures. The authors declare no conflicts of interest.

Data Availability. Data underlying the results presented in this paper are not publicly available at this time but may be obtained from the authors upon reasonable request.

Supplemental document. See Supplement 1 for supporting content.

REFERENCES

1. G. Armelles, A. Cebollada, A. García-Martín, and M. U. González, Adv. Opt. Mater. **1**, 10 (2013).
2. C. O. Avci, A. Quindeau, C.-F. Pai, M. Mann, L. Caretta, A. S. Tang, M. C. Onbasli, C. A. Ross, and G. S. D. Beach, Nat. Mater. **16**, 309 (2017).
3. J. Park, M. Inoue, J. Cho, K. Nishimura, and H. Uchida, J. Magn. **8**, 50 (2003).
4. G. A. Knyazev, P. O. Kapralov, N. A. Gusev, A. N. Kalish, P. M. Vetoshko, S. A. Dagesyan, and V. I. Belotelov, ACS Photon. **5**, 4951 (2018).
5. S. David, C. Polonschii, C. Luculescu, M. Gheorghiu, S. Gäspär, and E. Gheorghiu, Biosens. Bioelectron. **63**, 525 (2015).
6. B. Sepulveda, A. Calle, L. Lechuga, and G. Armelles, Opt. Lett. **31**, 1085 (2006).
7. J. N. Anker, W. P. Hall, O. Lyandres, N. C. Shah, J. Zhao, and R. P. Van Duyne, in *Nanoscience and Technology: A Collection of Reviews from Nature Journals* (2010), p. 308.
8. K. Fang, Z. Yu, V. Liu, and S. Fan, Opt. Lett. **36**, 4254 (2011).
9. N. Maccaferri, L. Bergamini, M. Pancaldi, M. K. Schmidt, M. Kataja, S. van Dijken, N. Zabala, J. Aizpurua, and P. Vavassori, Nano Lett. **16**, 2533 (2016).
10. A. N. Kalish, R. S. Komarov, M. A. Kozhaev, V. G. Achanta, S. A. Dagesyan, A. N. Shaposhnikov, A. R. Prokopov, V. N. Berzhansky, A. K. Zvezdin, and V. I. Belotelov, Optica **5**, 617 (2018).
11. P. K. Sahoo, S. Sarkar, and J. Joseph, Sci. Rep. **7**, 1 (2017).
12. A. N. Kalish, D. O. Ignatyeva, V. I. Belotelov, L. E. Kreilkamp, I. A. Akimov, A. V. Gopal, M. Bayer, and A. P. Sukhorukov, Laser Phys. **24**, 094006 (2014).
13. I. Razdolski, D. Makarov, O. G. Schmidt, A. Kirilyuk, T. Rasing, and V. V. Temnov, ACS Photon. **3**, 179 (2016).
14. V. I. Belotelov, I. A. Akimov, M. Pohl, V. A. Kotov, S. Kasture, A. S. Vengurlekar, A. V. Gopal, D. R. Yakovlev, A. K. Zvezdin, and M. Bayer, Nat. Nanotechnol. **6**, 370 (2011).
15. A. L. Chekhov, V. L. Krutyanskiy, A. N. Shaimanov, A. I. Stognij, and T. V. Murzina, Opt. Express **22**, 17762 (2014).
16. M. Levy, O. V. Borovkova, C. Sheidler, B. Blasiola, D. Karki, F. Jomard, M. A. Kozhaev, E. Popova, N. Keller, and V. I. Belotelov, Optica **6**, 642 (2019).
17. O. Borovkova, A. Kalish, and V. Belotelov, Opt. Lett. **41**, 4593 (2016).
18. O. V. Borovkova, H. Hashim, M. A. Kozhaev, S. A. Dagesyan, A. Chakravarty, M. Levy, and V. I. Belotelov, Appl. Phys. Lett. **112**, 063101 (2018).
19. O. V. Borovkova, H. Hashim, D. O. Ignatyeva, M. A. Kozhaev, A. N. Kalish, S. A. Dagesyan, A. N. Shaposhnikov, V. N. Berzhansky, V. G. Achanta, L. V. Panina, A. K. Zvezdin, and V. I. Belotelov, Phys. Rev. B **102**, 081405 (2020).
20. K. Y. Bliokh, F. J. Rodríguez-Fortuño, A. Y. Bekshaev, Y. S. Kivshar, and F. Nori, Opt. Lett. **43**, 963 (2018).
21. A. V. Chetvertukhin, A. A. Grunin, A. V. Baryshev, T. V. Dolgova, T. V. H. Uchida, M. Inoue, and A. A. Fedyanin, J. Magn. Magn. Mater. **324**, 3516 (2012).
22. A. Temiryazev, Diam. Relat. Mater. **48**, 60 (2014).
23. S. V. Tomilin and A. S. Yanovsky, J. Nano- Electron. Phys. **5**, 03014 (2013).
24. A. E. Khramova, D. O. Ignatyeva, M. A. Kozhaev, S. A. Dagesyan, V. N. Berzhansky, A. N. Shaposhnikov, S. V. Tomilin, and V. I. Belotelov, Opt. Express **27**, 33170 (2019).
25. A. Tseng, K. Chen, C. Chen, and K. Ma, IEEE Trans. Electron. Packag. Manuf. **26**, 141 (2003).
26. A. L. Chekhov, V. L. Krutyanskiy, V. A. Ketsko, A. I. Stognij, and T. V. Murzina, Opt. Mater. Express **5**, 1647 (2015).
27. K. Yin, D. Chu, X. Dong, C. Wang, J.-A. Duan, and J. He, Nanoscale **9**, 14229 (2017).
28. X. Gao, W. Feng, Z. Zhu, Z. Wu, S. Li, S. Kan, X. Qiu, A. Guo, W. Chen, and K. Yin, Adv. Mater. Interfaces **8**, 2002133 (2021).
29. J. S. Wi, R. J. Wilson, R. M. White, and S. X. Wang, J. Vac. Sci. Technol. B **29**, 033001 (2011).
30. E. Molotokaite, M. Gedvilas, G. Raciukaitis, and V. Girdauskas, J. Laser Micro/Nanoeng. **5**, 74 (2010).
31. M. Gedvilas, J. Mikšys, and G. Račiukaitis, RSC Adv. **5**, 75075 (2015).
32. V. I. Belotelov, D. A. Bykov, L. L. Doskolovich, A. N. Kalish, and A. K. Zvezdin, J. Exp. Theor. Phys. **110**, 816 (2010).